Supplementary Information

Yann Waltenspühl[1,2], Janosch Ehrenmann[1,3,#], Santiago Vacca[1,#], Cristian Thom[1,#], Ohad Medalia[1] and Andreas Plückthun[1*]

[1] *Department of Biochemistry, University of Zürich, Winterthurerstrasse 190, CH-8057 Zürich, Switzerland.*

[2]*Present address: Novo Nordisk A/S, Novo Nordisk Park 1, DK-2760 Måløv, Denmark*

[3]*Present address: leadXpro AG, PARK innovAARE, CH-5234 Villigen, Switzerland*

#These authors contributed equally: Janosch Ehrenmann, Santiago Vacca, Cristian Thom

[*]*Correspondence and requests for materials should be addressed to A.P. (plueckthun@bioc.uzh.ch*

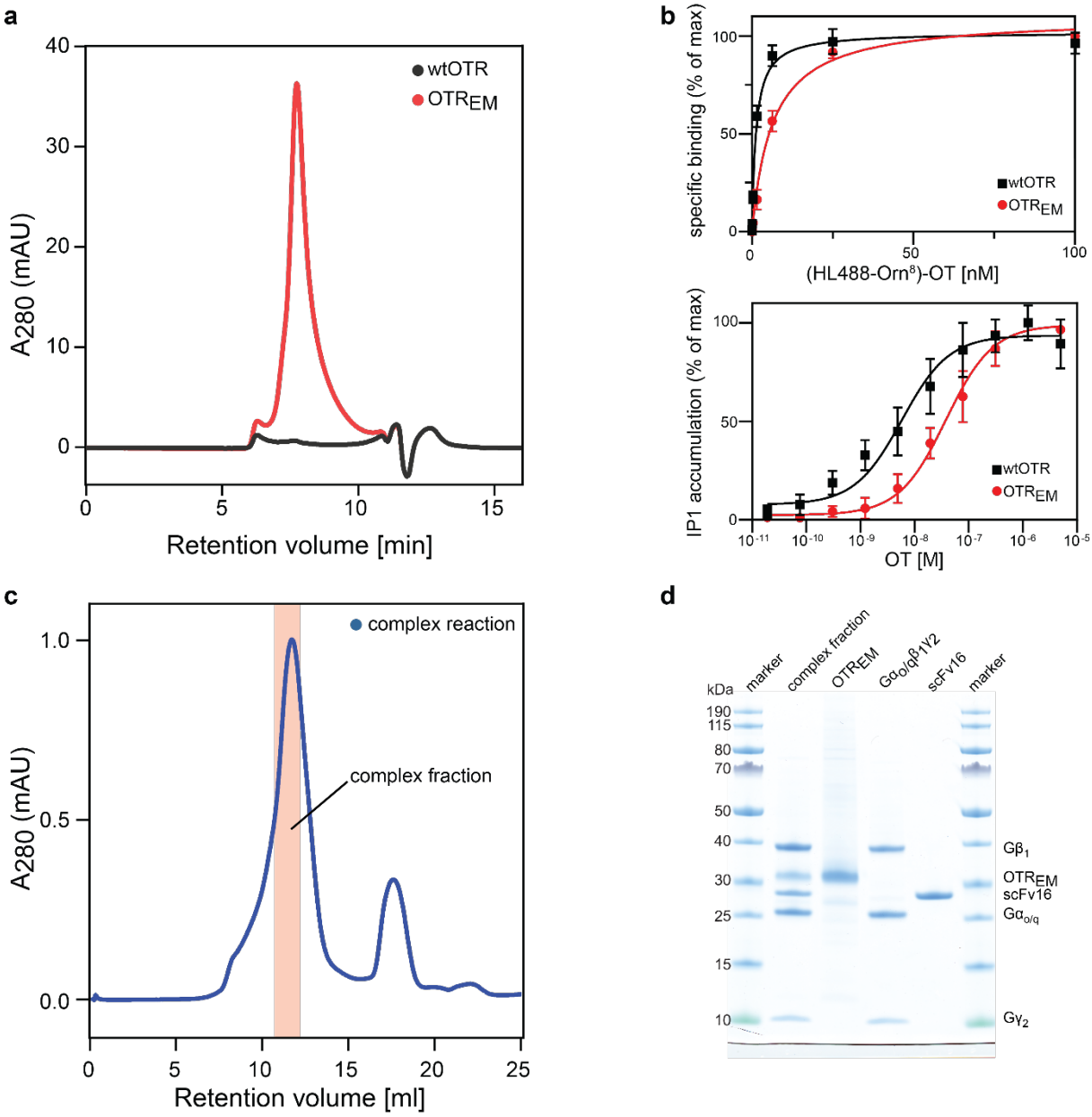

Supplementary Fig. 1 Purification of OTR_{EM} & complex formation.

a Small-scale analytical size-exclusion chromatography (SEC) profiles from initial purifications of wtOTR (black curve) and OTR-D153Y termed OTR_{EM} (red curve). SEC profiles present fair loads. **b** Agonist profiles of wtOTR and OTR_{EM}. Dose-response curves were obtained from IP1 accumulation assays, and saturation binding assays were measured by whole-cell ligand binding assays. Saturation binding curves are shown with mean ± standard deviation from six (wtOTR) or three (OTR_{EM}) independent experiments performed in triplicates. IP1 dose response curves are shown with mean ± standard deviation from six (wtOTR) or two (OTR_{EM}) independent experiments performed in duplicates. Source data are

provided as a Source Data file. **c** SEC profile of the OTR:OT:$G_{o/q}$:scFv16 complex. The red rectangle highlights the pooled fraction used for cryo-EM analysis. **d** LDS-PAGE gel of the pooled complex fraction and the single components.

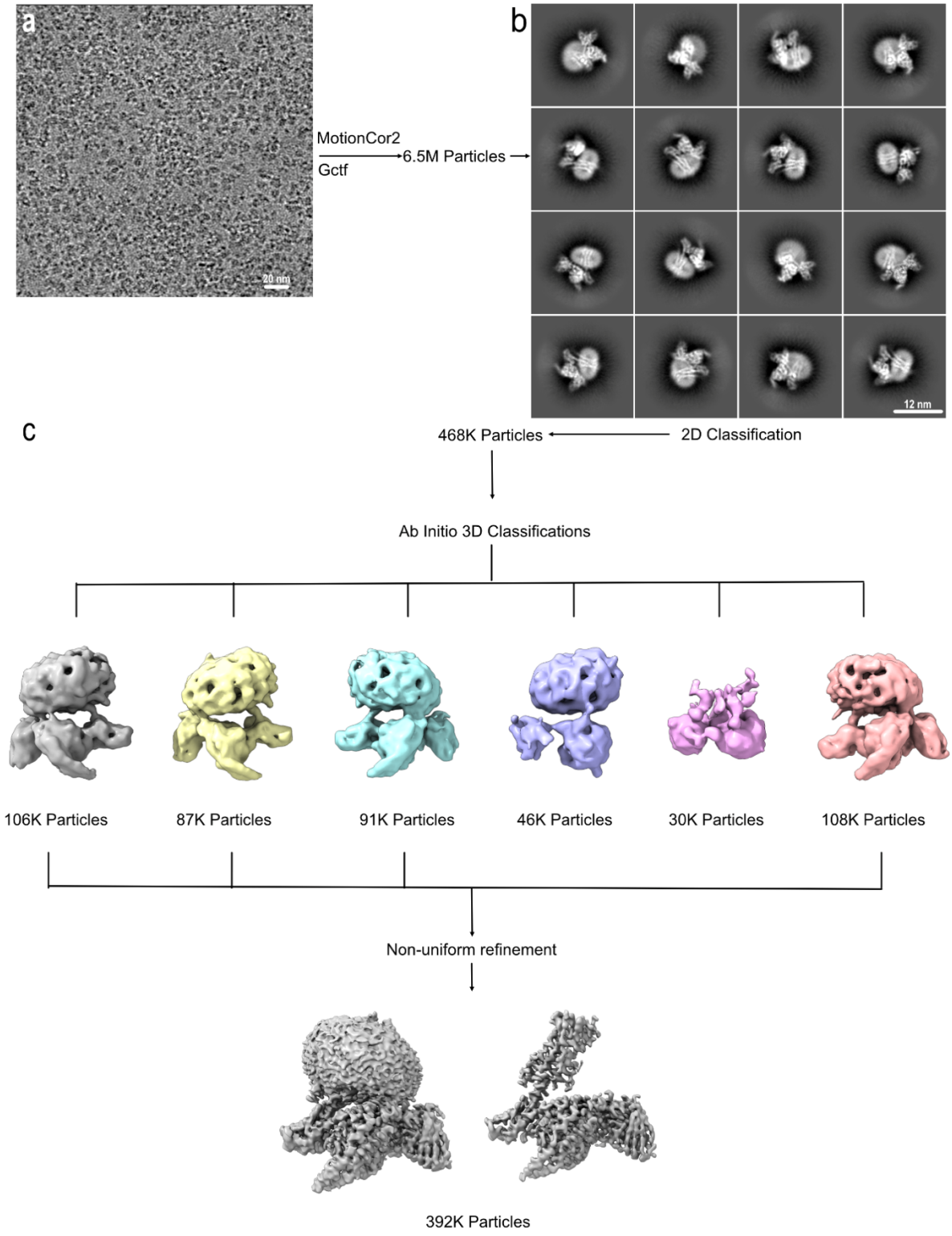

Supplementary Fig. 2 Overview of single-particle cryo-EM data processing.

a A representative cryo-EM micrograph of the 11,667 movie stacks of the OTR:OT:$G_{o/q}$:scFv16 complex. Scale bar, 20 nm. **b** Representative 2D averages showing distinct secondary structure features from different views of the complex. **c** 3D classification workflow and refinement.

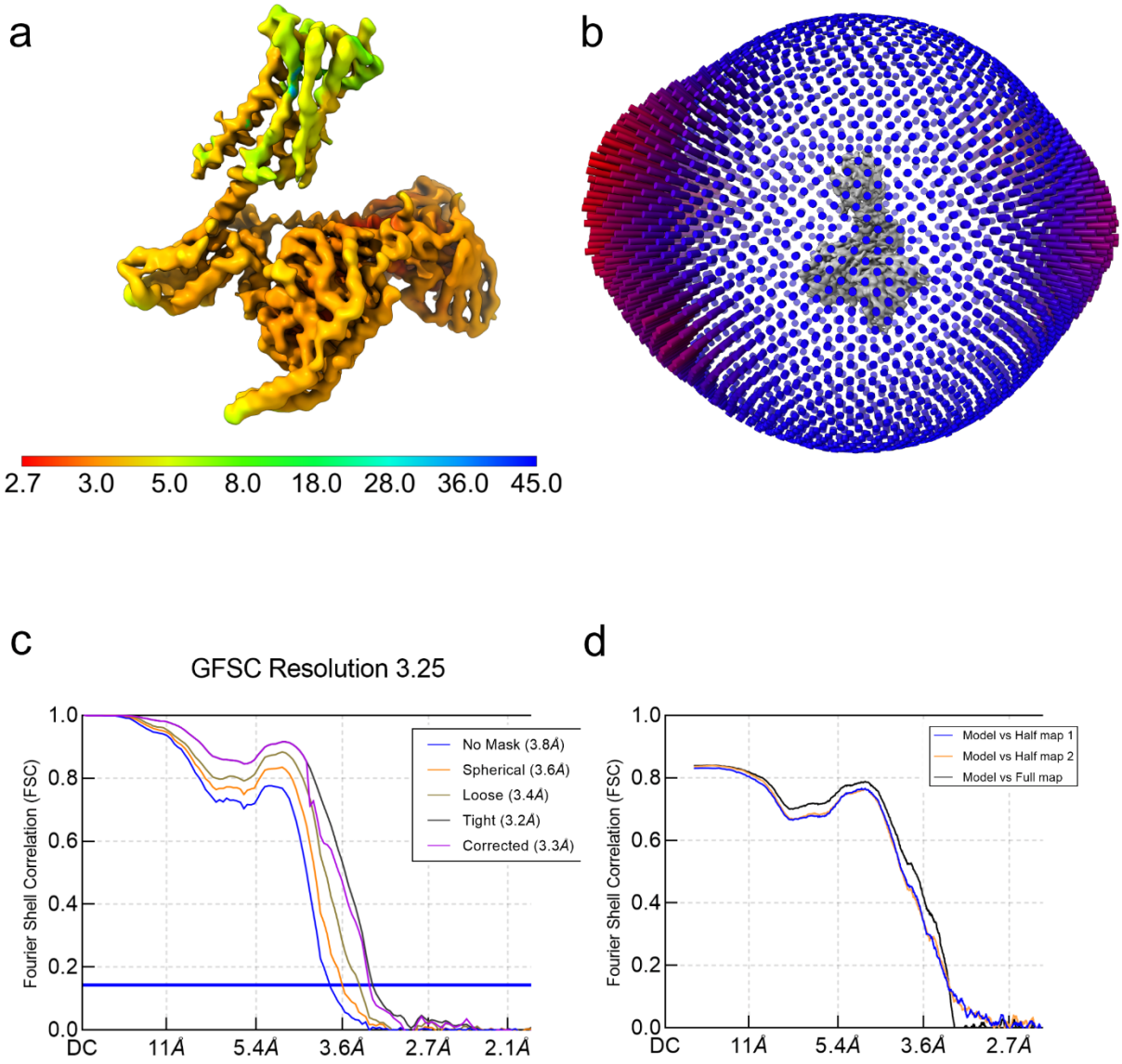

Supplementary Fig. 3 Resolution of the OTR:OT:$G_{o/q}$:scFv16 complex.

a Local resolution analysis of the OTR:OT:$G_{o/q}$:scFv16 complex. **b** Angular distribution of the particle orientations of the OTR:OT:$G_{o/q}$:scFv16 complex. **c** The gold-standard Fourier shell correlation curves for the map of the OTR:OT:$G_{o/q}$:scFv16 complex. **d** For cross-validation, FSC curves of the refined model versus full map (black), refined map versus half map 1 (blue), and refined model versus half map 2 (orange) were calculated.

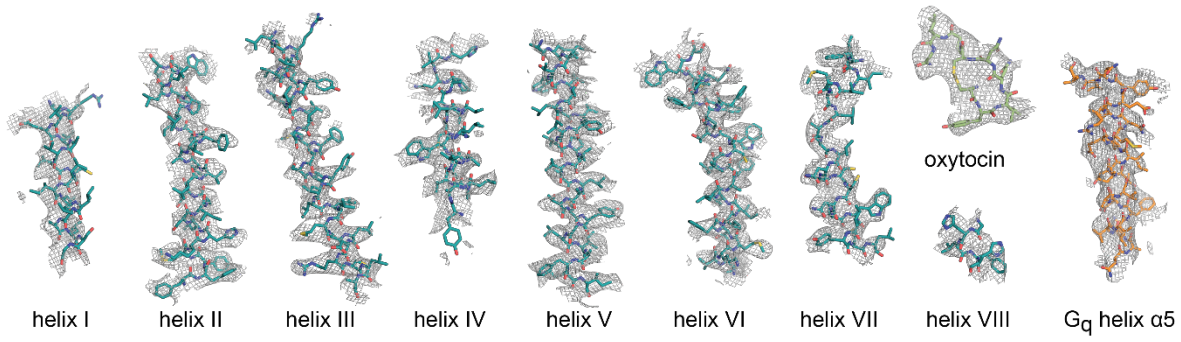

Supplementary Fig. 4 Cryo-EM density within OTR.

Cryo-EM density maps for all OTR transmembrane helices, helix VIII, oxytocin, and the interacting G_q α5 helix of the G protein.

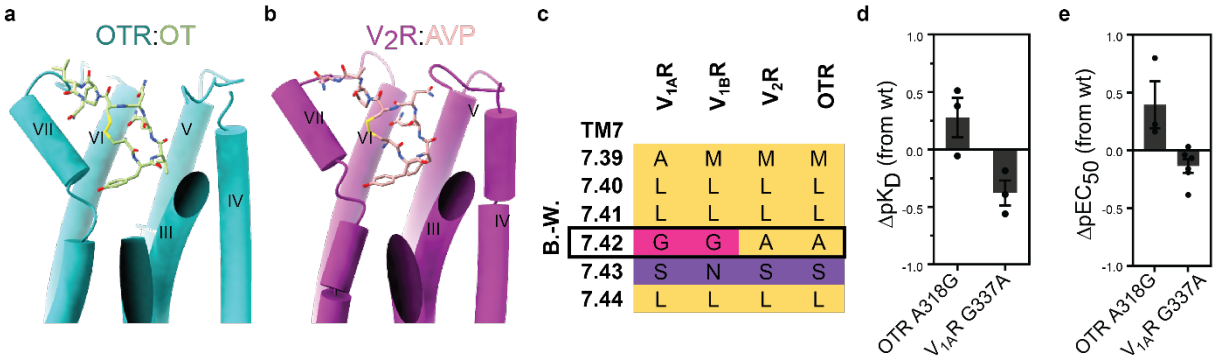

Supplementary Fig. 5 Conserved activation mechanism by oxytocin and vasopressin.

a Cylindrical representation of active OTR:OT complex with close-up on kink in helix VII. **b** Cylindrical representation of active V_2R:AVP complex (PDB ID: 7DW9 [https://www.rcsb.org/structure/7DW9]) with close-up on kink in helix VII. **c** Amino acid sequence alignment of the kink region for all human oxytocin and vasopressin receptors. Amino acid positions are denoted in Ballesteros-Weinstein numbering (B.-W.).**d** OT affinity profiles of OTR and V_{1A}R kink region mutants. Bars represent differences in affinity of the cognate ligand (mean pK_D ± SEM from three independent experiments in triplicates) compared to wtOTR or wtV_{1A}R. Source data are provided as a Source Data file. **e** OT IP1 accumulation dose-response curves of OTR and V_{1A}R kink region mutants. Bars represent differences in IP1 accumulation potency of the cognate ligand (mean pEC_{50} ± SEM from three (OTR A318G) or six (V_{1A}R G337A) independent transfections in duplicates) compared to wtOTR or wtV_{1A}R. Source data are provided as a Source Data file.

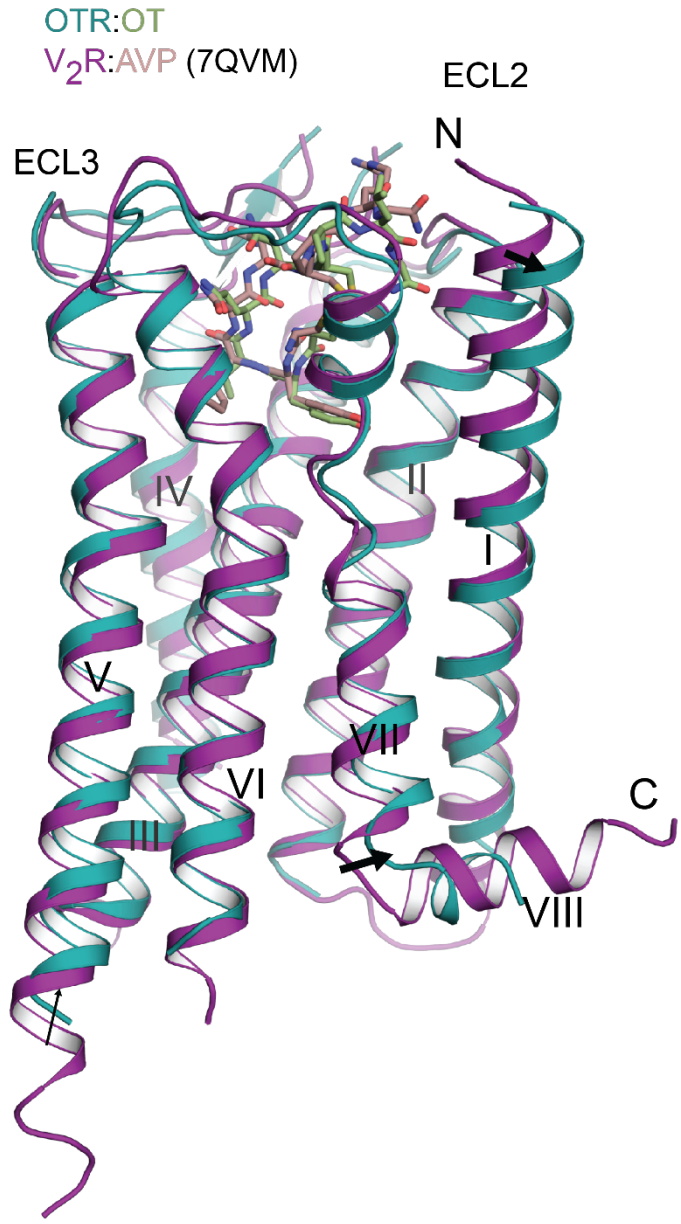

Supplementary Fig. 6 Comparison of the OTR and V_2R.

Structural superposition of the OTR:OT with V_2R:AVP (PDB ID: 7QVM [https://www.rcsb.org/structure/7DW9], illustrating the main differences between active OTR and V_2R. Arrows indicate the main differences in helix positioning and length.

Supplementary Table 1 Single-particle cryo-EM statistics.

	OTR:OT:$G_{o/q}$:scFv16 PDB ID: 7QVM
Data collection	
Microscope	Titan Krios G3i
Detector	Gatan K3
Energy filter slit width (eV)	20
Magnification	130,000
Voltage (kV)	300
Electron exposure ($e^-/Å^2$)	63.7
Defocus range (μm)	0.8-2.4
Pixel size (Å)	0.65
Symmetry imposed	C1
Number of Micrographs	11,667
Initial particle images (no.)	6.5 Mio
Final particle images (no.)	392,369
Map resolution (Å)	3.25
FSC threshold	0.143
Refinement	
Number of atoms	
All	8,551
Protein	8,482
Ligand	69
Model validation	
CC map vs. model (%)	76
RMSD	
Bond lengths (Å)	0.27
Bond angles (°)	0.640
Ramachandran statistics	
Favored regions (%)	96.4
Allowed regions (%)	3.5
Outliers (%)	0.0
Rotamer outliers (%)	0.0
C-beta deviations (%)	0.0
Clashscore	11.4
MolProbity overall score	1.8

Supplementary Table 2 Effects of mutations on OT-induced IP1-accumulation.

construct	EC_{50} [nM]	ΔpEC_{50}	E_{max} (% of wt)	n
wtOTR	8.4 ± 4	-	100	6
OTR_{EM}	42.9 ± 17	-0.52 ± 0.18	229 ± 29	2
Q92A	222.3 ± 141	-1.72 ± 0.28	12 ± 1	3
Q96A	1540 ± 286.3	-2.75 ± 0.05	68 ± 13	3
K116A	6.1 ± 0.8	-0.36 ± 0.03	48 ± 5	3
Q119A	444.3 ± 192.6	-2.15 ± 0.16	107 ± 33	3
M123A	n.a.	-	(1 ± 1)	3
Q171A	992.5 ± 180	-2.56 ± 0.04	90 ± 12	3
Q171N	39.1 ± 10.2	-1.14 ± 0.1	74 ± 11	3
F175A	3482 ± 857.7	-3.09 ± 0.07	66 ± 12	3
W188A	155.7 ± 62	-1.08 ± 0.18	85 ± 9	2
I201A	89.5 ± 15.4	-1.52 ± 0.12	22 ± 7	3
I204A	n.a.	-	(-2 ± 4)	3
F291A	541.8± 179.4	-1.63± 0.51	28 ± 7	2
F292A	6.1 ± 3.3	0.36 ± 0.62	9 ± 1	2
Q295A	51.3 ± 3.1	-0.63 ± 0.34	32 ± 1	2
L316A	21.9 ± 10.7	-0.21 ± 0.13	18 ± 4	2
A318G	4.6 ± 0.7	0.39 ± 0.2	50 ± 2	3
$wtV_{1A}R$	157.8 ± 27.6	-	100	6
G337A	249.7 ± 90.5	-0.14 ± 0.06	215 ± 15	6

HTRF-based measurements of IP1 accumulation in HEK293T cells expressing wild-type and mutated receptor variants. Activation curves were analyzed by fitting each experiment separately to a three-parameter logistic equation. All values are expressed as mean ± SEM of the indicated number of independent experiments performed in duplicate. n.a., no activation. Source data are provided as a Source Data file.

Supplementary Table 3 Effects of mutations on OT binding.

construct	K_D [nM]	ΔpK_D	B_{max} (% of wt)	n
wtOTR	1.4 ± 0.2	0	100	6
OTR_{EM}	6.4 ± 0.7	-0.6 ± 0.1	252 ± 10	3
A318G	0.9 ± 0.2	0.28 ± 0.17	28 ± 5	3
$wtV_{1A}R$	9.3 ± 2.2	0	100	3
G337A	20.9 ± 0.2	-0.38 ± 0.11	165 ± 23	3

Whole-cell specific saturation binding experiment of fluorescently labelled peptide OT-HL488 to HEK293T cells expressing wild-type and mutated receptor variants. Binding curves were analyzed by fitting each experiment separately to a one-site saturation binding equation. All values are expressed as mean ± SEM of the indicated number of independent experiments performed in triplicate. B_{max} values indicate the amount of functional receptor. Source data are provided as a Source Data file.